



Published in final edited form as:

IEEE Trans Biomed Eng. 2012 March ; 59(3): 706–716. doi:10.1109/TBME.2011.2178241.

Nonlinear Dynamic Modeling of Neuron Action Potential Threshold During Synaptically Driven Broadband Intracellular Activity

Ude Lu, IEEE [Member],

Department of Biomedical Engineering, Center for Neural Engineering, University of Southern California, Los Angeles, CA 90089 USA

Shane M. Roach, IEEE [Student Member],

Department of Neuroscience, University of Southern California, Los Angeles, CA 90089 USA

Dong Song, IEEE [Member], and

Department of Biomedical Engineering, Center for Neural Engineering, University of Southern California, Los Angeles, CA 90089 USA

Theodore W. Berger, IEEE [Fellow]

Department of Biomedical Engineering, Center for Neural Engineering, University of Southern California, Los Angeles, CA 90089 USA

Ude Lu: ulu@usc.edu; Shane M. Roach: shaneroa@usc.edu; Dong Song: dsong@usc.edu; Theodore W. Berger: berger@bmsr.usc.edu

Abstract

Activity-dependent variation of neuronal thresholds for action potential (AP) generation is one of the key determinants of spike-train temporal-pattern transformations from presynaptic to postsynaptic spike trains. In this study, we model the nonlinear dynamics of the threshold variation during synaptically driven broadband intracellular activity. First, membrane potentials of single CA1 pyramidal cells were recorded under physiologically plausible broadband stimulation conditions. Second, a method was developed to measure AP thresholds from the continuous recordings of membrane potentials. It involves measuring the turning points of APs by analyzing the third-order derivatives of the membrane potentials. Four stimulation paradigms with different temporal patterns were applied to validate this method by comparing the measured AP turning points and the actual AP thresholds estimated with varying stimulation intensities. Results show that the AP turning points provide consistent measurement of the AP thresholds, except for a constant offset. It indicates that 1) the variation of AP turning points represents the nonlinearities of threshold dynamics; and 2) an optimization of the constant offset is required to achieve accurate spike prediction. Third, a nonlinear dynamical third-order Volterra model was built to describe the relations between the threshold dynamics and the AP activities. Results show that the model can predict threshold accurately based on the preceding APs. Finally, the dynamic threshold model was integrated into a previously developed single neuron model and resulted in a 33% improvement in spike prediction.

Index Terms

Neuron; threshold dynamics; Volterra kernels; whole-cell patch-clamp

I. Introduction

Neurons receive inputs in the form of presynaptic action potentials (APs, or “spikes”) and transform them into post-synaptic APs. APs are all-or-none electrical events generated by a neuron that propagate down its axon. Since the amplitude of an AP contains little or no information, the temporal pattern of APs must play an essential role in encoding neural information [1]–[6]. Therefore, the characteristics of neuron spike-train to spike-train temporal transformation is critical to the various functions performed by nervous systems, such as learning and memory [7], [8]. Unraveling this neuron spike-train temporal transformation is fundamental to the understanding of the information processing done by nervous systems [9].

Neuron threshold is the transmembrane voltage level at which any further depolarization will activate a sufficient number of sodium channels to enter a self-generative positive-feedback phase (AP initiation). Variation of the threshold may significantly affect neuron spike-train temporal transformation [10]–[14]. Nevertheless, in many neuron models that have an explicit threshold term, e.g., integrate-and-fire models, threshold is often assumed to be a constant [8], [15]–[19]. However, more and more evidence shows that threshold is not constant but rather is influenced by the AP firing history in a nonlinear dynamical manner [10]–[12], [14]. The importance of threshold dynamics in affecting spike generation can be recognized in some recently developed neuron models that adopted more realistic spike initiation mechanisms to replace constant voltage threshold and showed significant improvement in spike prediction [13], [20]–[22]. One major possible mechanism for this history dependence is the voltage-dependent sodium channel which has been shown to undergo a slow accumulative inactivation process which is modulated by activation history [23], [24]. This report describes the development of a nonlinear model that is used to quantify and study the nonlinear dynamics of neuronal threshold as a function of AP firing history. There are four major stages of the model development: 1) the collection of synaptically activated subthreshold and suprathreshold intracellular activity driven by a broadband input; 2) a method to consistently measure threshold; 3) a data-driven modeling methodology to quantify threshold dynamics as a function of AP activity; and 4) the comparison of spike prediction performance made by the dynamical threshold model versus a constant threshold model.

A. Intracellular Responses to Presynaptic Broadband Inputs

The temporal transformation of spike trains between synaptically coupled neurons is a complex process that involves changes in pre- and post-synaptic conductance, dendritic and somatic integration, and AP generation [25], [26], among other mechanisms. These processes affect the activation and inactivation of voltage-dependent ion channels in a nonlinear manner. In order to study threshold dynamics under the widest range of nonlinear interactions of the underlying processes, random-interval impulse trains (RITs) of single all-or-none pulses were delivered to the synaptic region of CA1 stratum radiatum containing Schaffer collaterals. The all-or-none stimulation pulses mimic APs. The interspike intervals (ISIs) of the RITs follow a broadband distribution. These stimuli can elicit a broad range of physiologically plausible responses and nonlinearities resulting from the interactions of the underlying processes [3], [8], [27].

B. Threshold Measurement

In order to study threshold dynamics, we need an algorithm to consistently measure neuron threshold in a continuous record of neuron membrane potential. The physiological definition of neuron threshold is straightforward: the voltage level of membrane potential at which any

further depolarization will induce a sufficient number of sodium channel to enter a positive-feedback phase (AP initiation); however, to computationally obtain this voltage level from a continuous intracellular recording is not straightforward. Different algorithms have been developed to measure threshold [12], [14], [28]–[33]. Those algorithms aim to find the point at the base of the AP where the membrane potential increases at its fastest rate, referred to as the “AP turning point” in this report. Since this turning point is defined phenomenologically instead of following the physiological definition of threshold, this assumption might be problematic. This study applies various stimulation paradigms to examine the relation between the two.

C. Nonlinear Modeling Methodology

A data-driven modeling methodology is needed to capture the nonlinear threshold dynamics in response to the AP activity. Volterra modeling theory is a data-driven modeling methodology that canonically describes and quantifies nonlinear dynamical systems using progressively higher order kernels [5], [34], [35]. A third-order Volterra model was, thus, developed with AP timings as input, and the resultant threshold values as output (see Fig. 1). Response functions can be calculated from the Volterra kernels to provide intuitive physiological explanations of the threshold nonlinearities in terms of single-pulse, paired-pulse, and triple-pulse effects [36]–[39]. This dynamic threshold model requires minimal assumptions, which largely avoids errors resulting from incomplete and/or biased knowledge [5], [37], [38].

D. Comparison of Spike Prediction Accuracy Performed by Constant and Dynamical Threshold Models

A single neuron model was previously developed based on the principles of signal generation common to all spike-input spike-output neurons [36]. The signal generation is implemented by the model in three recurrent steps: 1) the model transforms presynaptic spikes to postsynaptic potentials; 2) if the postsynaptic potential is higher than the threshold, an AP is generated; 3) then, a spike-dependent after potential is triggered to modify subsequent postsynaptic potentials. The original threshold term of the model was a constant and it is replaced with the dynamic threshold developed in this study. The spike prediction accuracy performed by the two methods is statistically compared.

II. Materials and Methods

A. Experimental Procedures

Hippocampal slices (400 μm thick) were prepared from two-week-old male Sprague Dawley rats using standard protocols. A surgical disruption of the connection between CA3 and CA1 was performed on each slice before it was transported to oxygenated bath solution for maintenance at 25 $^{\circ}\text{C}$. This disruption was performed to prevent spontaneous activities in CA1 neurons driven by CA3 neurons. The bath solution contained (in millimolar): NaCl 128, KCl 2.5, NaH_2PO_4 1.25, NaHCO_3 26, Glucose 10, MgSO_4 1, Ascorbic Acid 2, and CaCl_2 2; at pH 7.4 and 295 mosmol.

During whole-cell patch-clamp recording, hippocampal slices were perfused with oxygenated bath solution at 25 $^{\circ}\text{C}$. Experiments were performed on pyramidal cells of the hippocampal CA1 system. A bipolar stimulation electrode was placed in the CA1 stratum radiatum according to visual cues; the stratum radiatum contains many glutamatergic, excitatory afferents to CA1 pyramidal cells, which are among the strongest and well studied of the inputs to CA1 from CA3 pyramidal neurons. The stimulation electrode was created using formvarinsulated Nichrome wire (A-M Systems, Inc., Carlsborg, WA). A recording micropipette electrode with a 4-M Ω tip resistance was patched on the somatic membrane of

a CA1 pyramidal neuron to record the intracellular postsynaptic potentials (PSPs) and APs. The internal solution of the recording electrode contained (in millimolar): Potassium-Gluconate 110, HEPES 10, EGTA 1, KCl 20, NaCl 4, Mg-ATP 2, and Na₃-GTP 0.25; at pH 7.3 and 290 mosmol.

A programmable stimulator (Multi Channel Systems MCS GmbH, Reutlingen, Germany) was used to deliver Poisson RITs with a 2-Hz mean frequency with the ISIs ranging from 10 to 4500 ms [40]–[44]. Whole-cell, patch-clamp recordings were performed with a HEKA EPC9/2 amplifier in a 20-kHz sampling rate. The stimulation intensities of spike trains were adjusted so that approximately 50% of the stimulations induced APs. This study includes 38 cells from 32 animals.

B. Measuring AP Turning Point and Threshold

The AP turning point is phenomenologically defined as that point at the base of the AP where the membrane potential increases at its fastest rate. The mathematical measurement of this AP turning point can be accomplished in different ways. We utilized the third-order derivative method suggested by Henze and Buzsáki in 2001 [12]. They suggested that the timing of the AP turning point is the same as the first peak of the third-order derivative of the membrane potential (see Fig. 2). The third-order derivative of the membrane potential is calculated as follows [45]:

$$\frac{d^3 V_t}{dt^3} \approx \frac{V_{t-3} - 8V_{t-2} + 13V_{t-1} - 13V_{t+1} + 8V_{t+2} - V_{t+3}}{8\Delta t^3}. \quad (1)$$

In (1), V represents membrane potential (in millivolt) and t represents time (in millisecond).

However, this phenomenologically defined AP turning point might not be the same as the physiologically defined neuron threshold. To examine the relationship between the two, four stimulation paradigms with different temporal patterns were applied: 1) single pulse, 2) paired pulse with 25-ms ISI, 3) paired pulse with 90-ms ISI, and 4) triple pulse with 90 and 25 ms ISIs (see Section III-A). Based on the findings, we then propose a two-step method to estimate the neuron threshold: 1) measure the AP turning point and 2) estimate the offset by optimizing spike prediction performance.

C. Dynamic Threshold Model

1) *Estimation of Dynamic Threshold Model Parameters:* In Fig. 1, y_h , the input spike trains (APs) to the dynamic threshold model, can be expressed in delta functions (spikes) as follows:

$$y_h(t) = \sum_{i=1}^N \delta(t - t_i) \quad (2)$$

where N is the total number of APs in a given sample and t_i is the time of the i th AP. The threshold value θ is the output of the dynamic threshold model and can be expressed as follows [5], [34]:

$$\theta(t) = (c_{\theta_1} - f) + \sum_{j=1}^L c_{\theta_2}(j) v_j^{\theta_2}(t) + \sum_{j_1=1}^L \sum_{j_2=1}^{j_1} c_{\theta_3}(j_1, j_2) v_{j_1}^{\theta_3}(t) v_{j_2}^{\theta_3}(t) \quad (3)$$

where L is the total number of Laguerre basis functions, c_{θ} are Laguerre coefficients estimated with least squares estimations as in (5), f is the constant offset between the AP

turning point and the threshold, which is optimized by minimizing spike prediction error rate (SPER) defined in (19) by scanning through possible voltage ranges [see Fig. 3(a)], and $v_j^\theta(t)$ are the convolutions of Laguerre basis functions and y_h expressed as follows:

$$v_j^\theta(t) = \sum_{\substack{i=1 \\ t-M_\theta < t_i < t}}^N b_j^\theta(t-t_i) \quad (4)$$

where b_j^θ represents Laguerre basis functions, and M_θ is a memory window sufficiently longer than threshold dynamics.

The least squares estimation for Laguerre coefficients c_θ in (3) is expressed as follows:

$$\begin{bmatrix} c_{\theta_1} \\ c_{\theta_2}(1) \\ \vdots \\ c_{\theta_2}(p) \\ c_{\theta_3}(1) \\ \vdots \\ c_{\theta_3}(q) \end{bmatrix}_{(1+p+q) \times 1} = \left[(V^T V)^{-1} V^T \right]_{(1+p+q) \times N} \begin{bmatrix} \tilde{\Theta}(1) \\ \tilde{\Theta}(2) \\ \vdots \\ \tilde{\Theta}(N) \end{bmatrix}_{N \times 1} \quad (5)$$

where $\tilde{\Theta}$ represents the measured AP turning points; p is the total number of second-order convolutions $[V_j^{\theta_2}]_{N \times 1}$; q is the total number of third-order convolutions $[V_{j_1}^{\theta_3} V_{j_2}^{\theta_3}]_{N \times 1}$; q is the concatenated matrix of all V_j^θ expressed as

$$V = \left[1, V_{j(1 \leq j \leq L)}^{\theta_2}, V_{j_1(1 \leq j_1 \leq L)}^{\theta_3}, V_{j_2(1 \leq j_2 \leq j_1)}^{\theta_3} \right]. \quad (6)$$

Fig. 3(b) shows the relationship between threshold and ISIs; it reveals that shorter ISIs are correlated with higher threshold values [11], [12]. Once the parameters of the dynamic threshold model are estimated, the model can predict the varying threshold values for each presynaptic input stimulation in x (see Fig. 4), which is expressed as

$$x(t) = \sum_{i=1}^N \delta(t-t_i). \quad (7)$$

A selection of representative threshold prediction made by the dynamic threshold model is shown in Fig. 3(c).

2) Reconstructions of Volterra Kernels and Response Functions: Volterra kernels were reconstructed with the estimated Laguerre coefficients c_θ , and the constant offset f , as follows:

$$k_1^\theta = c_{\theta_1} - f \quad (8)$$

$$k_{i,2 \leq i \leq 3}^\theta(m_1, \dots, m_{i-1}) = \sum_{j_1=1}^L \cdots \sum_{j_{i-1}=1}^{j_{i-2}} c_{\theta_{i-1}}(j_1, \dots, j_{i-1}) b_{j_1}^\theta(m_1) \cdots b_{j_{i-1}}^\theta(m_{i-1}) \quad (9)$$

where m_j are the intervals between current input events and preceding APs within the memory window.

To examine the threshold dynamics in terms of single-pulse, paired-pulse, and triple-pulse effects, we utilized response functions r . Response functions r can be calculated from Volterra kernels k as follows:

$$r_1 = k_1^\theta \quad (10)$$

$$r_2(m) = k_2^\theta(m) + k_3^\theta(m, m) \quad (11)$$

$$r_3(m_1, m_2) = 2k_3^\theta(m_1, m_2). \quad (12)$$

In (10), the first-order response function r_1 is a scalar, representing the expected threshold value of the current input (presynaptic stimulation) when there is no preceding AP within the memory window. In (11), the second-order response function r_2 is a curve, representing the nonlinear effect of threshold dynamics resulting from each preceding single AP with ISI equal to m . In (12), the third-order response function r_3 is a surface, representing the nonlinear effect on threshold resulting from each preceding pair of APs with ISIs equal to m_1 and m_2 .

D. Comparison of Spike Prediction Accuracy Produced by Constant and Dynamical Threshold Models

A single neuron model was previously developed based on principles of signal generation flow common to all spike-input, spike-output neurons [see Fig. 4(a)] [36]. It has three major components: 1) a feedforward model K transforming the presynaptic spikes x to PSPs u ; 2) a constant threshold term θ optimized by minimizing SPER, above which APs y_h are generated; and 3) a feedback model H describing spike-dependent after potentials a . The dynamic threshold model K^θ developed in this study was incorporated into this single neuron model to replace its original constant threshold term [see Fig. 4(b)]. Once the dynamic threshold model is estimated, meaning all open parameters are constrained using the synaptically driven intracellular activities, it predicts a varying threshold value θ for each incoming input stimulation x as a function of AP activity y_h .

The single neuron model shown in Fig. 4(a) and (b) can be expressed as follows:

$$w = u(K, x) + a(H, y_h) \quad (13)$$

$$y = \begin{cases} w + \text{action potential}, & w \geq \theta \\ w, & w < \theta. \end{cases} \quad (14)$$

In (13), x is the presynaptic stimulation train, as well as the input to the single neuron model; u represents PSP, the output of feedforward kernels; a represents spike-triggered after-potential, the output of feedback kernel; w represents the prethreshold (non-spiking) membrane potential, which is the summation of u and a . In (14), y is the overall continuous somatic membrane potential (both sub- and supra-threshold), and is also the output of the single neuron model; y_h represents the all-or-none spikes in y .

In (13) the PSP u is expressed with Volterra kernels as follows:

$$u(t) = c_{k_0} + \sum_{j=1}^L c_{k_1}(j) v_j^{k_1}(t) + \sum_{j_1=1}^L \sum_{j_2=1}^{j_1} c_{k_2}(j_1, j_2) v_{j_1}^{k_2}(t) v_{j_2}^{k_2}(t) + \sum_{j_1=1}^L \sum_{j_2=1}^{j_1} \sum_{j_3=1}^{j_2} c_{k_3}(j_1, j_2, j_3) v_{j_1}^{k_3}(t) v_{j_2}^{k_3}(t) v_{j_3}^{k_3}(t)$$

where

$$v_j^k(t) = \sum_{\tau=0}^{M_k} b_j^k(\tau) x(t - \tau). \quad (16)$$

In (15), L denotes the number of Laguerre basis functions; c_{k_0} , c_{k_1} , c_{k_2} , and c_{k_3} are the Laguerre expansion coefficients of the feedforward kernels k_0 , k_1 , k_2 , and k_3 shown in Fig. 4; M_k is the memory window.

In (13), a , spike-triggered after potential, is expressed with Volterra kernels as follows:

$$a(t) = \sum_{j=1}^L c_h(j) v_j^h(t) \quad (17)$$

where

$$v_j^h(t) = \sum_{\tau=1}^{M_h} b_j^h(\tau) y_h(t - \tau). \quad (18)$$

In (17), c_h are Laguerre expansion coefficients of the feedback kernel H ; M_h is the memory window.

1) *SPERs*: SPER is defined as follows:

$$\text{SPER} = \frac{\text{Number of False Positives} + \text{Number of False Negatives}}{\text{Total Number of Stimulations}}. \quad (19)$$

The SPER is used in this study as the spike prediction error measure to optimize the offset f between neuron threshold and AP turning point, as in (3) and in Fig. 3(a) for in-sample trainings. Hence, the SPER is used as the performance index for comparing the spike prediction accuracy performed by a constant threshold [see Fig. 4(a)] and the dynamic threshold model [see Fig. 4(b)] in out-of-sample predictions.

2) *Receiver Operating Characteristic (ROC) Curve*: An ROC curve is used in this study to visualize the significance of the improvement of spike prediction accuracy performed by the dynamic threshold model comparing to the constant threshold model. The x -axis of the ROC curve is false-positive rate and the y -axis is true-positive rate; they are defined as follows:

$$\text{False-Positives Rate} = \frac{\text{Number of False-Positives}}{\text{Number of Non-Spiking PSPs}} \quad (20)$$

$$\text{True-Positives Rate} = \frac{\text{Number of True-Positives}}{\text{Number of Spikes}}. \quad (21)$$

III. Results

A. Consistency of the Third-Order Derivative Analysis of Membrane Potentials With Different Temporal Patterns and the Relationship Between AP Turning Point and Threshold

We applied four stimulation paradigms to activate CA1 neurons in order to study: 1) whether or not the third-order derivative analysis provides a consistent measurement of AP turning points in response to different temporal patterns of prespike membrane potentials, and 2) the relationship between the phenomenologically defined AP turning point and the physiological neuron AP threshold. These four stimulation paradigms are 1) single-pulse stimulation, 2) paired-pulse stimulation with a 25-ms ISI, 3) paired-pulse stimulation with a 90-ms ISI, and 4) triple-pulse stimulation with 90- and 25-ms ISIs, in which an AP was evoked by the second pulse. In each stimulation pattern, the last stimulus has an increasing intensity ranging from 25 to 800 μ A. The measurements of the responses to the last stimulus, either the peak values of PSPs or turning points of APs, are plotted in the right column of Fig. 5.

In Fig. 5, notice that the AP turning points in each panel on the right remain relatively stable across different stimulation intensities. This stability shows that the third-order derivative analysis suggested by Henze and Buzsáki [12] provides reasonably consistent measurement of AP turning points in response to different temporal patterns of membrane potential evoked by various input patterns.

Recall the physiological definition of neuron threshold: the voltage level of membrane potential at which any further depolarization will activate a sufficient number of sodium channels to enter a positive-feedback phase. Under a certain stimulation intensity, if both nonspiking PSPs and APs coexist, then the average of the maximum peak values of the nonspiking PSPs represents the neuron threshold, which is plotted in each panel of the right column in Fig. 5.

In Fig. 5(a), the single-pulse stimulation paradigm was applied. This paradigm elicits the first-order PSP dynamics (no preceding presynaptic stimulation) and the first-order threshold dynamics (no preceding AP). The average normalized AP turning point is 109.8% (standard deviation (SD) = 5.1%); the average normalized threshold is 100% (SD = 4.23%), yielding an average of 9.8% difference. In Fig. 5(b), the paired-pulse stimulation paradigm with a 25-ms ISI was applied. This paradigm elicits the second-order PSP dynamics (one preceding presynaptic stimulation) and the first-order threshold dynamics (no preceding AP). Hence, 25 ms is the peak time of a single PSP response. The average normalized AP turning point is 109.4% (SD = 3.19%); the average normalized threshold is 97% (SD = 2.01%), yielding an average of 12.4% difference. In Fig. 5(c), the paired-pulse stimulation paradigm with a 90-ms ISI was applied. This paradigm elicits the second-order PSP dynamics (one preceding presynaptic stimulation) and the first-order threshold dynamics (no preceding AP). Hence, 90 ms is the time interval at which the strongest paired-pulse (second-order) PSP facilitation occurs [36]. The average normalized AP turning point is 108.1% (SD = 4.88%); the average normalized threshold is 97.3% (SD = 2.94%), yielding an average of 10.8% difference. In Fig. 5(d), the triple-pulse stimulation paradigm was applied with 90- and 25-ms ISIs in which an AP was evoked by the second stimulus. This pattern elicits the third-order PSP dynamics (two preceding presynaptic stimulations) and the second-order threshold dynamics (one preceding AP). The average normalized AP turning point is 135% (SD = 7.94%); the average normalized threshold is 122.5% (SD = 1.44%), yielding an average of 12.5% difference. Notice that the threshold is about 23% higher than the previous three stimulation paradigms. This elevation in threshold is caused by the previous AP activity. This phenomenon is congruent with Figs. 3(b) and 6(b).

The analyses in Fig. 5 show that, in this specific neuron, there is an approximately 10% offset between AP turning points and thresholds (9.8–12.5% differences across all four patterns). This offset relationship suggests that there is a relatively constant voltage shift between the actual potential level at which sufficient sodium channel activation enters the neuron into the positive-feedback phase (AP initiation) and the potential level at which the drastic increase in membrane potential can be observed phenomenologically (AP rise).

Among all CA1 neurons collected in this study, AP turning points are always larger than thresholds. However, the offset value is different from cell to cell, and needs to be optimized on an individual basis. The offset relationship indicates that AP turning point captures the nonlinearities but not the linearity of threshold dynamics. From a neuroscience standpoint, this offset may not be specially significant. However, from a neuroengineering standpoint, accurate estimation of this offset bears a very significant weight to the spike prediction accuracy. In recognition of this, we propose a two-step methodology to estimate the neuron threshold: 1) apply the third-order derivative analysis introduced in Section II-B, to measure AP turning point, and 2) perform a spike prediction validation to optimize the offset between AP turning point and neuron threshold.

B. Threshold Dynamics

A set of representative response functions (r_1 , r_2 , and r_3) are shown in Fig. 6. The first-order response function r_1 is 8.9 mV. The second-order response function r_2 is a double-positive-peak curve and stays positive throughout the memory window. The first peak starts from amplitude 5.18 mV at the beginning and decays to 0.30 mV at $m = 225$ ms. The second peak ranges from $m = 225$ to 1200 ms with maximum amplitude 0.59 mV at $m = 490$ ms. The third-order response function r_3 starts from -0.09 mV, symmetrically decays to the first valley of -1.1 mV at (40ms, 160 ms) and (160 ms, 40ms), rises to the highest peak of 0.31 mV at (160 ms, 160 ms), decays to the second valley of -0.4 mV at (400 ms, 400 ms), and then slowly rises back to -0.01 mV at (800 ms, 800 ms).

The first-order response function indicates that 8.9 mV is the expected threshold value in the case when there is no preceding APs within the memory window. The second-order response function is positive throughout the memory window, and higher value corresponds with shorter m (ISI); this indicates the general phenomena also observed in Fig. 3(b): the second AP in a pair requires a stronger driving force, and higher threshold corresponds with shorter ISI. However, Fig. 6(b) is more informative and conclusive than Fig. 3(b), because Fig. 3(b) considers only one single spike prior to the second spike, whereas Fig. 6(b) (second-order response function) considers all possible pairing spikes within the memory window prior to the second spike. Taking a step further, Fig. 6(c) (third-order response functions) considers all possible triplets within the memory window. In summary, the response functions in Fig. 6 provide a quantitative description of the linearity and nonlinearities of threshold dynamics.

C. Improvement of the SPER by the Integration of the Dynamic Threshold Model

Two representative out-of-sample spike predictions performed using either constant threshold or dynamic threshold are compared in Fig. 7. Fig. 7(a) shows predictions in which constant threshold accurately predicted the occurrences of APs; the dynamic threshold worked just as well, i.e., dynamic threshold did not worsen the SPER values. Fig. 7(b) shows that predictions of the constant threshold made three false-positives errors; however, the dynamic threshold mode avoided two out of the three errors, notably improving the spike prediction accuracy.

Fig. 8(a) shows the ROC curves made using a constant threshold by scanning through the possible voltage range of threshold and using the dynamic threshold model by scanning through the possible voltage range of the offset. The difference between the two curves shows that the dynamic threshold model significantly enhances the spike prediction performance comparing to a constant threshold. Histograms of out-of-sample SPERs made using an optimal constant threshold and dynamic threshold with optimal offset are shown in Fig. 8(b). The mean SPER made using an optimal constant threshold is 24.8%, and using a dynamic threshold is 14.7%. The average out-of-sample SPER improvement made using the dynamic threshold model over the constant threshold is 33% [see Fig. 8(c)]. This significant SPER improvement affirms the importance of the activity-dependent threshold dynamics in influencing the neuron spike-train temporal-pattern transformations.

IV. Discussion

In this study, we developed a data-driven, high-order, nonlinear dynamic model to quantify the activity-dependent threshold dynamics induced by presynaptic broadband stimulation. The developed dynamic threshold model quantitatively describes the transformation from AP activity (input) to threshold dynamics (output). The input and the output of the model are common to all spiking neurons, meaning the model is applicable to various kinds of spike-input, spike-output neurons. All parameters of this dynamic threshold model are simultaneously estimated using synaptically driven intracellular activity by minimizing rigorously defined error terms. This data-driven approach provides the following methodological advantages: 1) avoiding arbitrary manipulation during parameter estimation; 2) requiring minimal assumptions about the model; and 3) considering only fundamental constraints general to all neurons [9], [36], [38], [39], [46]. Therefore, modeling errors due to biased knowledge or unknown mechanisms are reduced. In addition, this dynamic threshold model is computationally efficient. It contains only 11 open parameters (i.e., one parameter for the first-order Volterra kernel, three for the second-order, six for the third-order, and one for the offset) and can be easily estimated using a standard PC (AMD Phenom 9750).

This study affirms the importance of threshold dynamics in neuron spike-train to spike-train transformation. This can be illustrated by the 33% average SPER improvement by dynamic threshold versus constant threshold [see Fig. 8(c)]. In other words, this marked improvement shows that threshold dynamics profoundly influence the input–output properties of neurons.

The single neuron model with the dynamic threshold [see Fig. 4(b)] decomposes neuron input–output dynamics into three principles: 1) the transformation from presynaptic spike to PSP; 2) spike generation with dynamic threshold; and 3) the transformation from output spike to spike-triggered after potential. The nonlinear dynamics of each principle are described using independent Volterra models. This model structure partitions the overall neuron input–output transformation according to the fundamental principles of neuronal signal generation, and, thus, significantly facilitates model interpretation and prediction [36], [46], [47].

The model is a hybrid, combining mechanistic and nonparametric representations. The model structure configuration is mechanistic, i.e., the principal underlying neurobiological processes (synaptic integration, spike generation, and spike-triggered after potential.) determine the global model structure. On the other hand, the transformations within each process are described in a nonparametric manner by Volterra models. In principle, including more mechanisms can make the model more biologically realistic and potentially more accurate. In practice, however, the availabilities of mechanistic dissection into nonparametrically modelable segments are dependent on the nature of experimentally

collected data. For example, we previously developed a single neuron model using extracellularly recorded unitary spikes as both the model input and model output [8], [47]. Since extracellular spike recording does not provide information about the prespike membrane potential, direct measurements of threshold cannot be performed and construction of a dynamic threshold model as reported was not possible. On the contrary, intracellularly recorded membrane potential provides enough information for direct measurement of threshold, and, thus, makes the inclusion of threshold dynamics possible. Nevertheless, that previous neuron model [8], [47] contains a spike-dependent feedback component describing the effects of spike-triggered after potentials. That feedback component groups the threshold dynamics and the spike-triggered after-potential dynamics into one entity, because spike-triggered after potential and threshold dynamics are both AP activity dependent. Obviously, intracellular recording contains richer neuronal information and allows a more in-depth decomposition of the system through a more mechanistic (parametric) model structure configuration [38], [39].

The mechanisms underlying activity-dependent threshold variation are likely to involve voltage-dependent ion channels. The fast, voltage-dependent sodium channel is one of the most likely candidates [11], [12], [48]–[51]. It has been reported that sodium channels in the soma and dendrites of CA1 pyramidal neurons undergo a form of AP use-dependent, cumulative inactivation that attenuates neuronal excitability [23], [24]. This cumulative inactivation of sodium channels makes the second AP in a pair more difficult to evoke within a certain time range than the first one. Thus, a stronger depolarizing force is needed for the second AP. This is observed in Figs. 3(b) and 6, where higher thresholds correlate with shorter ISIs. This spike-dependent attenuation in neuron excitability has been proposed to work as a noise filter that increases information transfer in nervous systems [14], and a coincidence detector that contributes to the synchronization among neurons [10], [11], [48]. Hence, this attenuation is also proposed to increase the homeostasis of the brain [52].

The reconstructed response functions shown in Fig. 6 describe threshold dynamics in terms of single-pulse, paired-pulse, and triple-pulse effects. Even though the response functions do not provide direct explanations of the physiological mechanisms underlying the threshold dynamics, they do provide valuable information for mechanistic hypotheses. In Fig. 6, the double-positive-peak curve in the second-order response function and the complex surface in the third-order response function suggest that at least two or more major processes interactively contribute to threshold dynamics. We propose that the dominant first peak of the second-order response function r_2 , where ISI (m) ranges from 0 to 225 ms, is due to sodium channel inactivation. Hence, there should be at least one additional process, e.g., an ionic channel, with a slower time constant that accounts for the second peak of r_2 where ISI (m) ranges from 225 to 1200 ms. Delayed-rectifier potassium channels may be one of the possible candidates [53]–[60]. Further experimental and modeling studies are required to identify the contributions of specific biological mechanisms to the overall response functions. For example, it would be useful to compare the response functions estimated from intracellular recordings both before and after pharmacologically blocking a specific ionic channel (e.g., sodium or potassium channel). In addition, we can compare the response functions estimated from the simulated data generated by a detailed compartmental CA1 neuron model before and after computationally blocking the same ionic channel. Subsequently, we can cross examine the experiment-derived- and the compartmental-model-derived response functions to segregate mechanism-specific contributions to the response functions and overall threshold dynamics.

Acknowledgments

This work was supported by the National Science Foundation (USC Biomimetic Microelectronic Systems Engineering Research Center), by the National Institute of Biomedical Imaging and Bioengineering (USC Biomedical Simulations Resource), and by the Office of Naval Research under Grant N00014-10-1-0685.

References

- Berger TW, Chauvet G, Sclabassi RJ. A biologically based model of functional properties of the hippocampus. *Neural Netw.* 1994; vol. 7(no. 6–7):1031–1064.
- Sclabassi RJ, Eriksson JL, Port RL, Robinson GB, Berger TW. Nonlinear systems analysis of the hippocampal perforant path-dentate projection. I. Theoretical and interpretational considerations. *J. Neurophysiol.* 1988 Sep.vol. 60(no. 3):1066–1076. [PubMed: 3171656]
- Berger TW, Eriksson JL, Ciarolla DA, Sclabassi RJ. Nonlinear systems analysis of the hippocampal perforant path-dentate projection. II. Effects of random impulse train stimulation. *J. Neurophysiol.* 1988 Sep.vol. 60(no. 3):1076–1094. [PubMed: 3171657]
- Berger TW, Eriksson JL, Ciarolla DA, Sclabassi RJ. Nonlinear systems analysis of the hippocampal perforant path-dentate projection. III. Comparison of random train and paired impulse stimulation. *J. Neurophysiol.* 1988 Sep.vol. 60(no. 3):1095–1109. [PubMed: 3171658]
- Marmarelis, VZ. *Nonlinear Dynamic Modeling of Physiological Systems.* Hoboken, NJ: Wiley-Interscience; 2004.
- Harris KD, Henze DA, Hirase H, Leinekugel X, Dragoi G, Czurkó A, Buzsáki G. Spike train dynamics predicts theta-related phase precession in hippocampal pyramidal cells. *Nature.* 2002 Jun.vol. 417(no. 6890):738–741. [PubMed: 12066184]
- Berger TW, Ahuja A, Courellis SH, Deadwyler SA, Erinjippurath G, Gerhardt GA, Gholmieh G, Granacki JJ, Hampson R, Hsaio MC, Lacoss J, Marmarelis VZ, Nasiatka P, Srinivasan V, Song D, Tanguay AR, Wills J. Restoring lost cognitive function. *IEEE Eng. Med. Biol. Mag.* 2005 Sep-Oct.vol. 24(no. 5):30–44. [PubMed: 16248115]
- Song D, Chan RHM, Marmarelis VZ, Hampson RE, Deadwyler SA, Berger TW. Nonlinear dynamic modeling of spike train transformations for hippocampal-cortical prostheses. *IEEE Trans. Biomed. Eng.* 2007 Jun.vol. 54(no. 6):1053–1066. [PubMed: 17554824]
- Berger TW, Song D, Chan RH, Marmarelis VZ. The neurobiological basis of cognition: Identification by multi-input, multioutput nonlinear dynamic modeling: A method is proposed for measuring and modeling human long-term memory formation by mathematical analysis and computer simulation of nerve-cell dynamics. *Proc. IEEE.* 2010 Mar.vol. 98(no. 3):356–374.
- Azouz R, Gray CM. Cellular mechanisms contributing to response variability of cortical neurons in vivo. *J. Neurosci.* 1999 Mar.vol. 19(no. 6):2209–2223. [PubMed: 10066274]
- Azouz R, Gray CM. Dynamic spike threshold reveals a mechanism for synaptic coincidence detection in cortical neurons in vivo. *Proc. Natl. Acad. Sci. USA.* 2000 Jul.vol. 97(no. 14):8110–8115. [PubMed: 10859358]
- Henze DA, Buzsaki G. Action potential threshold of hippocampal pyramidal cells in vivo is increased by recent spiking activity. *Neuroscience.* 2001; vol. 105(no. 1):121–130. [PubMed: 11483306]
- Kobayashi R, Tsubo Y, Shinomoto S. Made-to-order spiking neuron model equipped with a multi-timescale adaptive threshold. *Frontiers Comput. Neurosci.* 2009; vol. 3(no. 9)
- Chacron MJ, Lindner B, Longtin A. Threshold fatigue and information transfer. *J. Comput. Neurosci.* 2007 Dec.vol. 23(no. 3):301–311. [PubMed: 17436067]
- Geisler CD, Goldberg JM. A stochastic model of the repetitive activity of neurons. *Biophys. J.* 1966 Jan.vol. 6(no. 1):53–69. [PubMed: 19431343]
- Gerstner, W.; Kistler, W. *Spiking Neuron Models: Single Neurons, Populations, Plasticity.* Cambridge, U.K: Cambridge Univ. Press; 2002.
- Izhikevich EM. Simple model of spiking neurons. *IEEE Trans. Neural Netw.* 2003 Nov.vol. 14(no. 6):1569–1572. [PubMed: 18244602]

18. Koch C, Segev I. The role of single neurons in information processing. *Nature Neurosci.* 2000 Nov.vol. 3(Suppl. 1):1171–1177. [PubMed: 11127834]
19. Koch, C. *Biophysics of Computation: Information Processing in Single Neurons.* New York: Oxford Univ. Press; 2004.
20. Brette R, Gerstner W. Adaptive exponential integrate-and-fire model as an effective description of neuronal activity. *J. Neurophysiol.* 2005 Nov.vol. 94(no. 5):3637–3642. [PubMed: 16014787]
21. Ermentrout B. Type I membranes, phase resetting curves, and synchrony. *Neural Comput.* 1996 Jul.vol. 8(no. 5):979–1001. [PubMed: 8697231]
22. Fourcaud-Trocme N, Hansel D, van Vreeswijk C, Brunel N. How spike generation mechanisms determine the neuronal response to fluctuating inputs. *J. Neurosci.* 2003 Dec.vol. 23(no. 37): 11628–11640. [PubMed: 14684865]
23. Jung HY, Mickus T, Spruston N. Prolonged sodium channel inactivation contributes to dendritic action potential attenuation in hippocampal pyramidal neurons. *J. Neurosci.* 1997 Sep.vol. 17(no. 17):6639–6646. [PubMed: 9254676]
24. Mickus T, Jung H, Spruston N. Properties of slow, cumulative sodium channel inactivation in rat hippocampal CA1 pyramidal neurons. *Biophys. J.* 1999 Feb.vol. 76(no. 2):846–860. [PubMed: 9929486]
25. Hille, B. *Ion Channels of Excitable Membranes.* 3rd ed.. Sunderland, MA: Sinauer Associates; 2001.
26. Johnston, D.; Wu, SMS. *Foundations of Cellular Neurophysiology.* Cambridge, MA: MIT Press; 1995.
27. Gholmieh G, Courellis S, Marmarelis V, Berger T. An efficient method for studying short-term plasticity with random impulse train stimuli. *J. Neurosci. Methods.* 2002 Dec.vol. 121(no. 2):111–127. [PubMed: 12468002]
28. Sekerli M, Del Negro CA, Lee RH, Butera RJ. Estimating action potential thresholds from neuronal time-series: New metrics and evaluation of methodologies. *IEEE Trans. Biomed. Eng.* 2004 Sep.vol. 51(no. 9):1665–1672. [PubMed: 15376515]
29. Anderson P, Storm J, Wheal HV. Thresholds of action potentials evoked by synapses on the dendrites of pyramidal cells in the rat hippocampus in vitro. *J. Physiol.* 1987 Feb.vol. 383:509–526. [PubMed: 3656132]
30. Brownstone RM, Jordan LM, Kriellaars DJ, Noga BR, Shefchyk SJ. On the regulation of repetitive firing in lumbar motoneurons during fictive locomotion in the cat. *Exp. Brain Res.* 1992; vol. 90(no. 3):441–455. [PubMed: 1426105]
31. Krawitz S, Fedirchuk B, Dai Y, Jordan LM, McCrea DA. State-dependent hyperpolarization of voltage threshold enhances motoneurone excitability during fictive locomotion in the cat. *J. Physiol.* 2001 Apr.vol. 532(no. Pt 1):271–281. [PubMed: 11283241]
32. Dai Y, Jones KE, Fedirchuk B, McCrea DA, Jordan LM. A modelling study of locomotion-induced hyperpolarization of voltage threshold in cat lumbar motoneurons. *J. Physiol.* 2002 Oct.vol. 544(no. Pt 2):521–536. [PubMed: 12381824]
33. Porter JT, Johnson CK, Agmon A. Diverse types of interneurons generate thalamus-evoked feedforward inhibition in the mouse barrel cortex. *J. Neurosci.* 2001 Apr.vol. 21(no. 8):2699–2710. [PubMed: 11306623]
34. Marmarelis VZ. Identification of nonlinear biological systems using Laguerre expansions of kernels. *Ann. Biomed. Eng.* 1993 Nov-Dec;vol. 21(no. 6):573–589. [PubMed: 8116911]
35. Marmarelis VZ, Berger TW. General methodology for nonlinear modeling of neural systems with Poisson point-process inputs. *Math. Biosci.* 2005 Jul.vol. 196(no. 1):1–13. [PubMed: 15963534]
36. Lu D, Song D, Berger TW. Nonlinear dynamic modeling of synaptically driven single hippocampal neuron intracellular activity. *IEEE Trans. Biomed. Eng.* 2011 May.vol. 58(no. 5): 1303–1313. [PubMed: 21233041]
37. Song D, Marmarelis VZ, Berger TW. Parametric and nonparametric models of short-term plasticity. *Proc. 2nd Joint Eng. Med. Biol. Soc./Biomed. Eng. Soc. Conf.* 2002; vol. 3:1964–1965.
38. Song D, Marmarelis VZ, Berger TW. Parametric and non-parametric modeling of short-term synaptic plasticity. Part I: Computational study. *J. Comput. Neurosci.* 2009 Feb.vol. 26(no. 1):1–19. [PubMed: 18506609]

39. Song D, Wang Z, Marmarelis VZ, Berger TW. Parametric and non-parametric modeling of short-term synaptic plasticity. Part II: Experimental study. *J. Comput. Neurosci.* 2009 Feb.vol. 26(no. 1): 21–37. [PubMed: 18504530]
40. Barnes CA, McNaughton BL, Mizumori SJ, Leonard BW, Lin LH. Comparison of spatial and temporal characteristics of neuronal activity in sequential stages of hippocampal processing. *Prog. Brain Res.* 1990; vol. 83:287–300. [PubMed: 2392566]
41. Del Castillo J, Katz B. Quantal components of the end-plate potential. *J. Physiol.* 1954 Jun.vol. 124(no. 3):560–573. [PubMed: 13175199]
42. Hampson RE, Heyser CJ, Deadwyler SA. Hippocampal cell firing correlates of delayed-match-to-sample performance in the rat. *Behav. Neurosci.* 1993 Oct.vol. 107(no. 5):715–739. [PubMed: 8280383]
43. Softky WR, Koch C. The highly irregular firing of cortical cells is inconsistent with temporal integration of random EPSPs. *J. Neurosci.* 1993 Jan.vol. 13(no. 1):334–350. [PubMed: 8423479]
44. Tsodyks MV, Markram H. The neural code between neocortical pyramidal neurons depends on neurotransmitter release probability. *Proc. Natl. Acad. Sci. USA.* 1997 Jan.vol. 94(no. 2):719–723. [PubMed: 9012851]
45. Raton, B. *Standard Mathematical Tables and Formulae.* 29th ed.. Boca Raton, FL: CRC Press; 1991.
46. Song D, Chan RH, Marmarelis VZ, Hampson RE, Deadwyler SA, Berger TW. Nonlinear dynamic modeling of spike train transformations for hippocampal-cortical prostheses. *IEEE Trans. Biomed. Eng.* 2007 Jun.vol. 54(no. 6):1053–1066. [PubMed: 17554824]
47. Song D, Chan RH, Marmarelis VZ, Hampson RE, Deadwyler SA, Berger TW. Nonlinear modeling of neural population dynamics for hippocampal prostheses. *Neural Netw.* 2009 Nov.vol. 22(no. 9): 1340–1351. [PubMed: 19501484]
48. Azouz R, Gray CM. Adaptive coincidence detection and dynamic gain control in visual cortical neurons in vivo. *Neuron.* 2003 Feb.vol. 37(no. 3):513–523. [PubMed: 12575957]
49. Fricker D, Verheugen JA, Miles R. Cell-attached measurements of the firing threshold of rat hippocampal neurones. *J. Physiol.* 1999 Jun.vol. 517:791–804. [PubMed: 10358119]
50. Wilent WB, Contreras D. Stimulus-dependent changes in spike threshold enhance feature selectivity in rat barrel cortex neurons. *J. Neurosci.* 2005 Mar.vol. 25(no. 11):2983–2991. [PubMed: 15772358]
51. Platkiewicz J, Brette R. A threshold equation for action potential initiation. *PLoS Comput. Biol.* 2010; vol. 6(no. 7):e1000850. [PubMed: 20628619]
52. Buzsaki G, Csicsvari J, Dragoi G, Harris K, Henze D, Hirase H. Homeostatic maintenance of neuronal excitability by burst discharges in vivo. *Cereb. Cortex.* 2002 Sep.vol. 12(no. 9):893–899. [PubMed: 12183388]
53. Chi XX, Nicol GD. Manipulation of the potassium channel Kv1.1 and its effect on neuronal excitability in rat sensory neurons. *J. Neurophysiol.* 2007 Nov.vol. 98(no. 5):2683–2692. [PubMed: 17855588]
54. Murakoshi H, Trimmer JS. Identification of the Kv2.1K⁺ channel as a major component of the delayed rectifier K⁺ current in rat hippocampal neurons. *J. Neurosci.* 1999 Mar.vol. 19(no. 5): 1728–1735. [PubMed: 10024359]
55. Sanguinetti MC, Jurkiewicz NK. Two components of cardiac delayed rectifier K⁺ current. Differential sensitivity to block by class III antiarrhythmic agents. *J. Gen. Physiol.* 1990 Jul.vol. 96(no. 1):195–215. [PubMed: 2170562]
56. Goldberg EM, Clark BD, Zagha E, Nahmani M, Erisir A, Rudy B. K⁺ channels at the axon initial segment dampen near-threshold excitability of neocortical fast-spiking GABAergic interneurons. *Neuron.* 2008 May.vol. 58(no. 3):387–400. [PubMed: 18466749]
57. Guan D, Lee JC, Higgs MH, Spain WJ, Foehring RC. Functional roles of Kv1 channels in neocortical pyramidal neurons. *J. Neurophysiol.* 2007 Mar.vol. 97(no. 3):1931–1940. [PubMed: 17215507]
58. Kole MH, Letzkus JJ, Stuart GJ. Axon initial segment Kv1 channels control axonal action potential waveform and synaptic efficacy. *Neuron.* 2007 Aug.vol. 55(no. 4):633–647. [PubMed: 17698015]

59. Gittelman JX, Tempel BL. Kv1.1-containing channels are critical for temporal precision during spike initiation. *J. Neurophysiol.* 2006 Sep.vol. 96(no. 3):1203–1214. [PubMed: 16672305]
60. Shu Y, Yu Y, Yang J, McCormick DA. Selective control of cortical axonal spikes by a slowly inactivating K⁺ current. *Proc. Natl. Acad. Sci. U S A.* 2007 Jul.vol. 104(no. 27):11453–11458. [PubMed: 17581873]

Biographies



Ude Lu (S'05–M'11) received the B.S. degree in electrical and control engineering and the M.S. degree in biological science and technology from the National Chiao Tung University, Hsinchu, Taiwan, in 2000 and 2002, respectively, and the Ph.D. degree in biomedical engineering from the University of Southern California, Los Angeles, in 2011.

From 2002 to 2004, he was a Research Associate at the Institute of Biomedical Sciences of Academia Sinica, Taipei, Taiwan. He is currently in the Department of Biomedical Engineering, University of Southern California. His current research interests include nonlinear system analysis of single neuron, modeling input–output properties of neurological systems, electrophysiology of hippocampus, and long-term and short-term synaptic plasticity.

Dr. Lu is a member of the Biomedical Engineering Society and the Society for Neuroscience.



Shane M. Roach (S'11) received the B.A. degree (with distinction) in computer science from Carroll College, Helena, MT, in 2004. He is currently working toward the Ph.D. degree in neuroscience at the University of Southern California (USC), Los Angeles.

His current research interests include long-term synaptic plasticity and dendritic electrophysiology of the hippocampus, the neural basis of behavior, and direct neural interfaces.

Mr. Roach received the Tom Steward Award for Excellence in Computer Science in 2004. He is the recipient of the USC Neuroscience Graduate Program Merit Fellowship. He is a member of the Biomedical Engineering Society and the Society for Neuroscience.



Dong Song (S'02–M'04) received the B.S. degree in biophysics from the University of Science and Technology of China, Hefei, China, and the Ph.D. degree in biomedical engineering from the University of Southern California (USC), Los Angeles, in 1994 and 2003, respectively.

From 2004 to 2006, he was a Postdoctoral Research Associate at the Center for Neural Engineering, USC, where he is currently a Research Assistant Professor in the Department of Biomedical Engineering. His current research interests include nonlinear system analysis of nervous system, cortical neural prosthesis, electrophysiology of hippocampus, long-term and short-term synaptic plasticity, and the development of modeling methods incorporating both parametric and nonparametric modeling techniques.

Dr. Song is a member of the American Statistical Association, the Biomedical Engineering Society, and the Society for Neuroscience.



Theodore W. Berger (M'03–SM'04–F'09) received the Ph.D. degree from Harvard University, Cambridge, MA, in 1976.

From 1977 to 1978, he was a Postdoctoral Researcher at the University of California, Irvine. From 1978 to 1979, he was an Alfred P. Sloan Foundation Fellow at the Salk Institute. He joined the Departments of Neuroscience and Psychiatry, University of Pittsburgh, Pittsburgh, PA, in 1979, where he became a Full Professor in 1987. He is currently the David Packard Professor of engineering, a Professor of biomedical engineering and neuroscience, and the Director of the Center for Neural Engineering, University of Southern California (USC), where he has been a Professor of biomedical engineering and neurobiology since 1992, and became the David Packard Chair of Engineering in 2003. He has authored or coauthored more than 170 journal articles and book chapters. He is the coeditor of the book *Toward Replacement Parts for the Brain: Implantable Biomimetic Electronics as Neural Prostheses* (Cambridge, MA: MIT Press, 2005). In 1997, he became the Director of the Center for Neural Engineering, an organization that helps to unite USC faculty with cross-disciplinary interests in neuroscience, engineering, and medicine. His current research interests include the development of biologically realistic, experimentally based, mathematical models of higher brain (hippocampus) function, application of biologically realistic neural network models to real-world signal processing problems, very large-scale integration (VLSI)-based implementations of biologically realistic models of higher brain function, neuron–silicon interfaces for bidirectional communication between brain and VLSI systems, and next-generation brain-implantable, biomimetic signal processing devices for neural prosthetic replacement and/or enhancement of brain function.

Dr. Berger was the recipient of the James McKeen Cattell Award from the New York Academy of Sciences, the McKnight Foundation Scholar Award, and twice the National Institute of Mental Health (NIMH) Research Scientist Development Award. He was elected a Fellow of the American Association for the Advancement of Science. While at USC, he has received an NIMH Senior Scientist Award, was given the Lockheed Senior Research Award in 1997, was elected as a Fellow of the American Institute for Medical and Biological Engineering in 1998, received a Person of the Year “Impact Award” by the American Association of Retired Persons in 2004 for his research on neural prostheses, was

a National Academy of Sciences International Scientist Lecturer in 2003, and an IEEE Distinguished Lecturer during 2004–2005. He received a “Great Minds, Great Ideas” Award from the EE Times in 2005, and in 2006 was awarded USC’s Associates Award for Creativity in Research and Scholarship.

dynamic threshold model

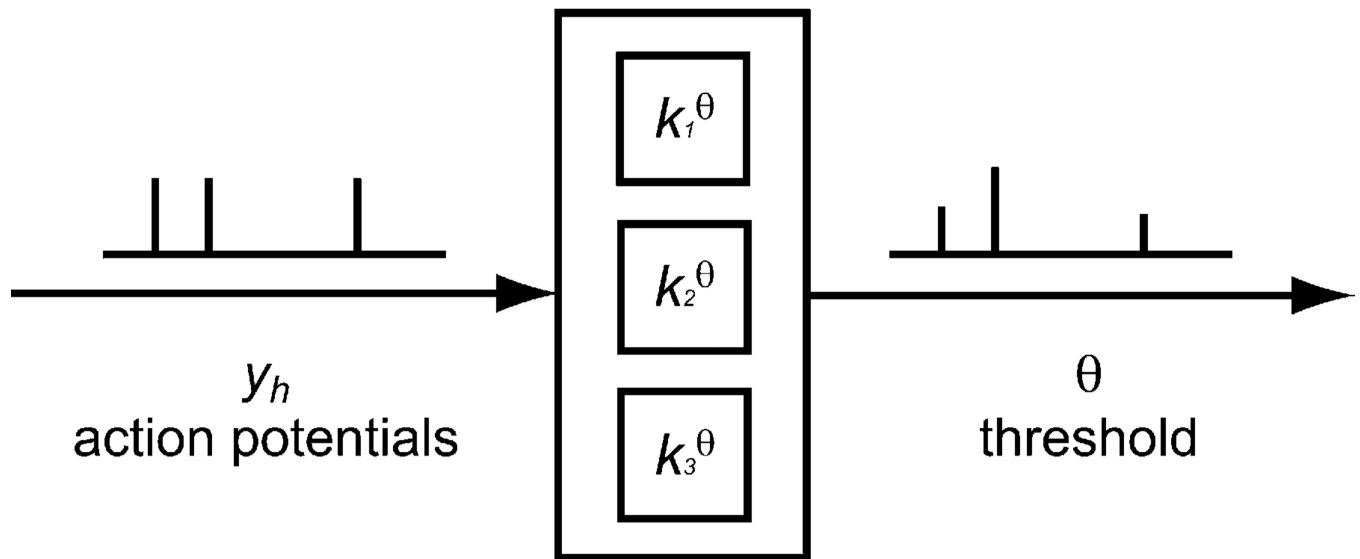


Fig. 1. Dynamic threshold model. The model is constructed using third-order Volterra kernels. The model canonically quantifies and describes the transformation between APs and thresholds. This also means that once the model parameters are trained, the model can predict threshold values as a function of AP firing history.

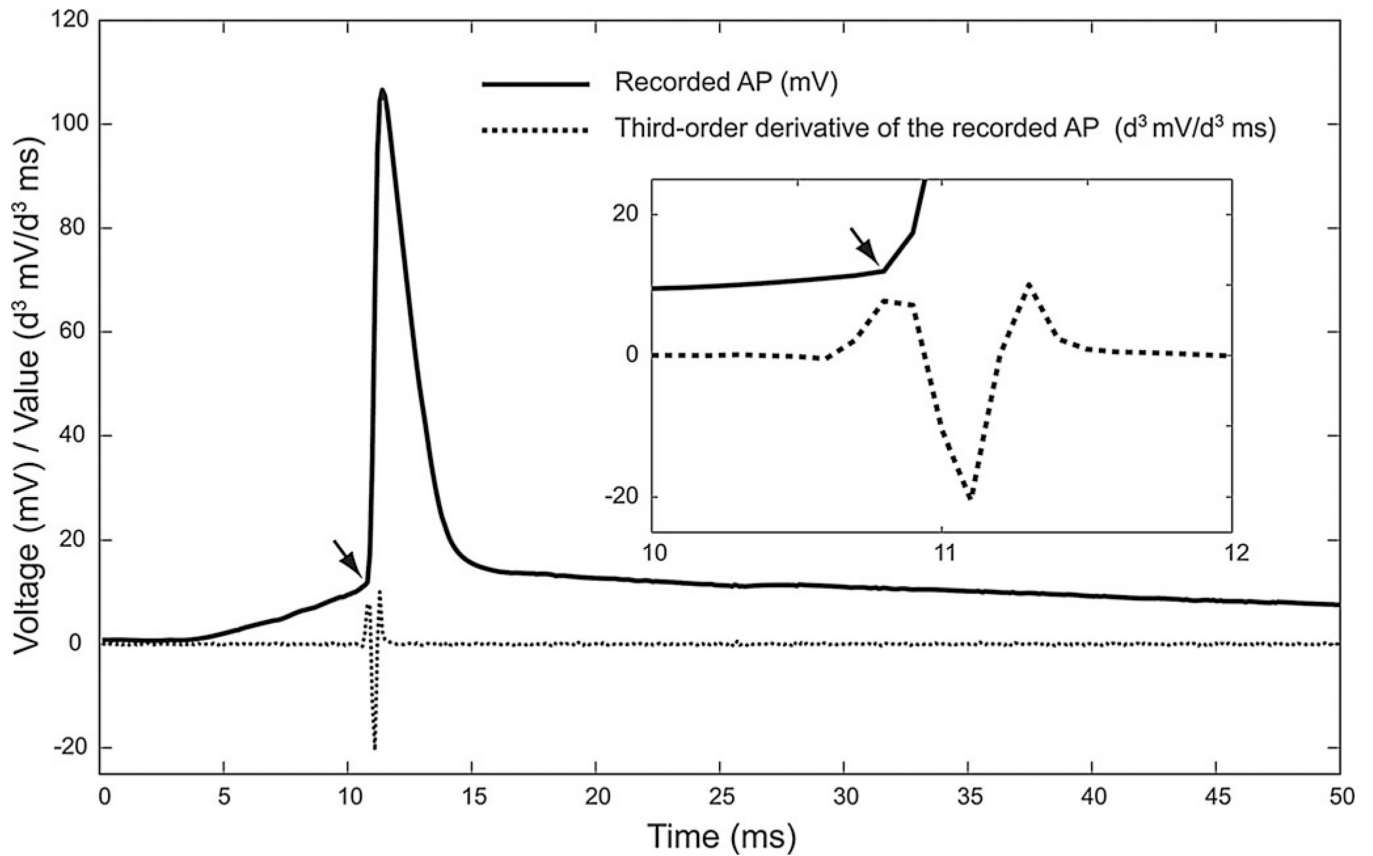
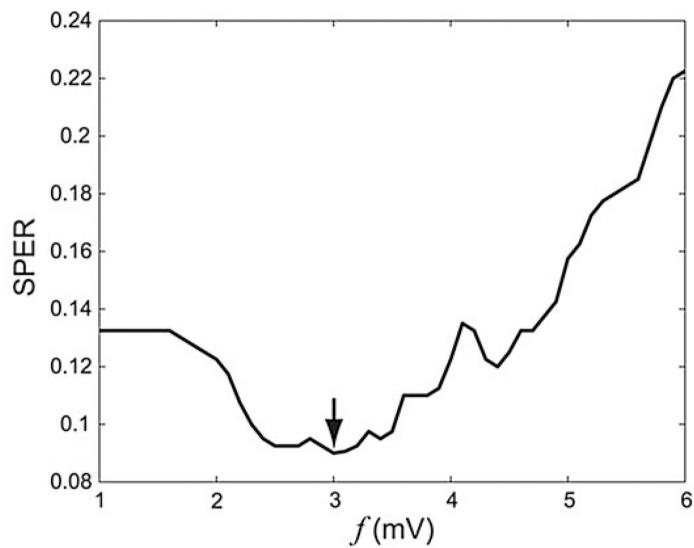
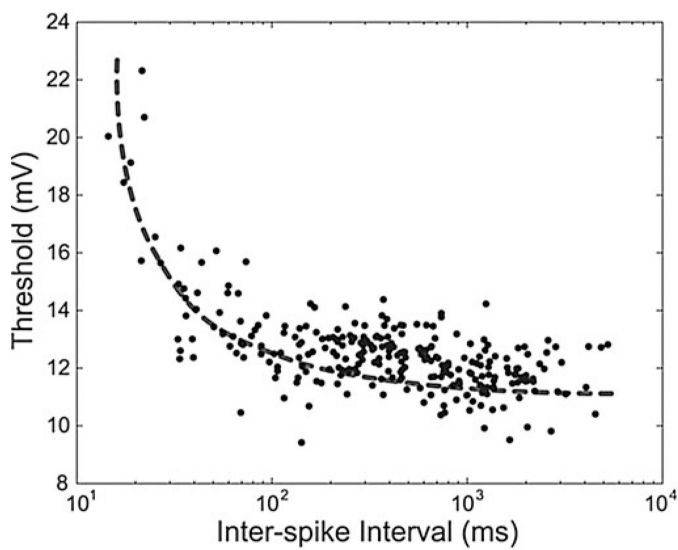


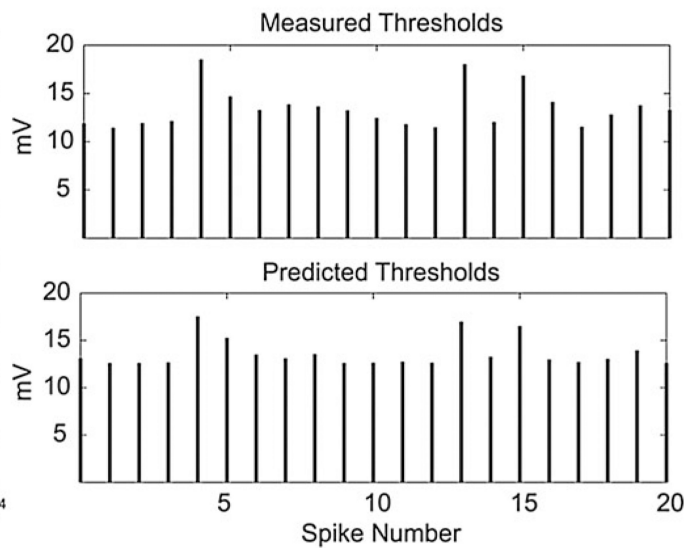
Fig. 2. Third-order derivative analysis of AP turning point. The solid line is the recorded membrane potential of an AP. The dashed line is its third-order derivative. Arrows indicate the AP turning point which happens at the same time point as the first peak of the third-order derivative.



(a)



(b)



(c)

Fig. 3. (a) Optimization of the offset f by scanning through possible voltage range to minimize the SPER. This offset is further discussed in Section III. (b) Measured threshold versus ISI. It shows that previous spiking activity generally increases the threshold value of the following spikes, while shorter ISI correlates with higher threshold value. (c) Representative threshold predictions made by the dynamic threshold model.

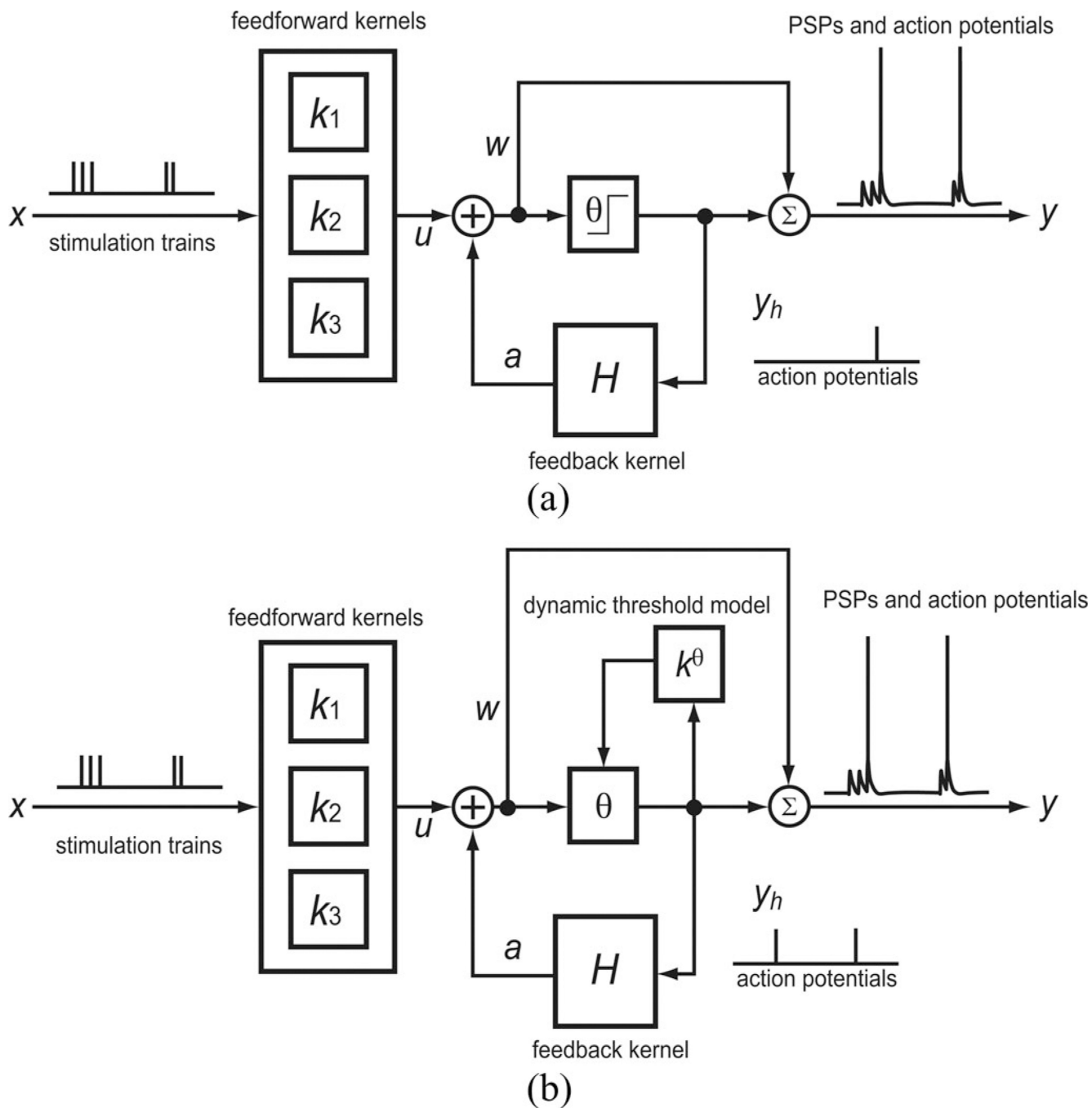


Fig. 4. Model structure of the single neuron model with (a) a constant threshold and (b) the dynamic threshold model. In this model, x represents presynaptic stimulations; u represents PSPs; w represents prethreshold PSP; θ represents either constant threshold in (a) or dynamic threshold in (b); y_h represents APs; a represents spike-dependent after potentials. Σ is defined as superimposition.

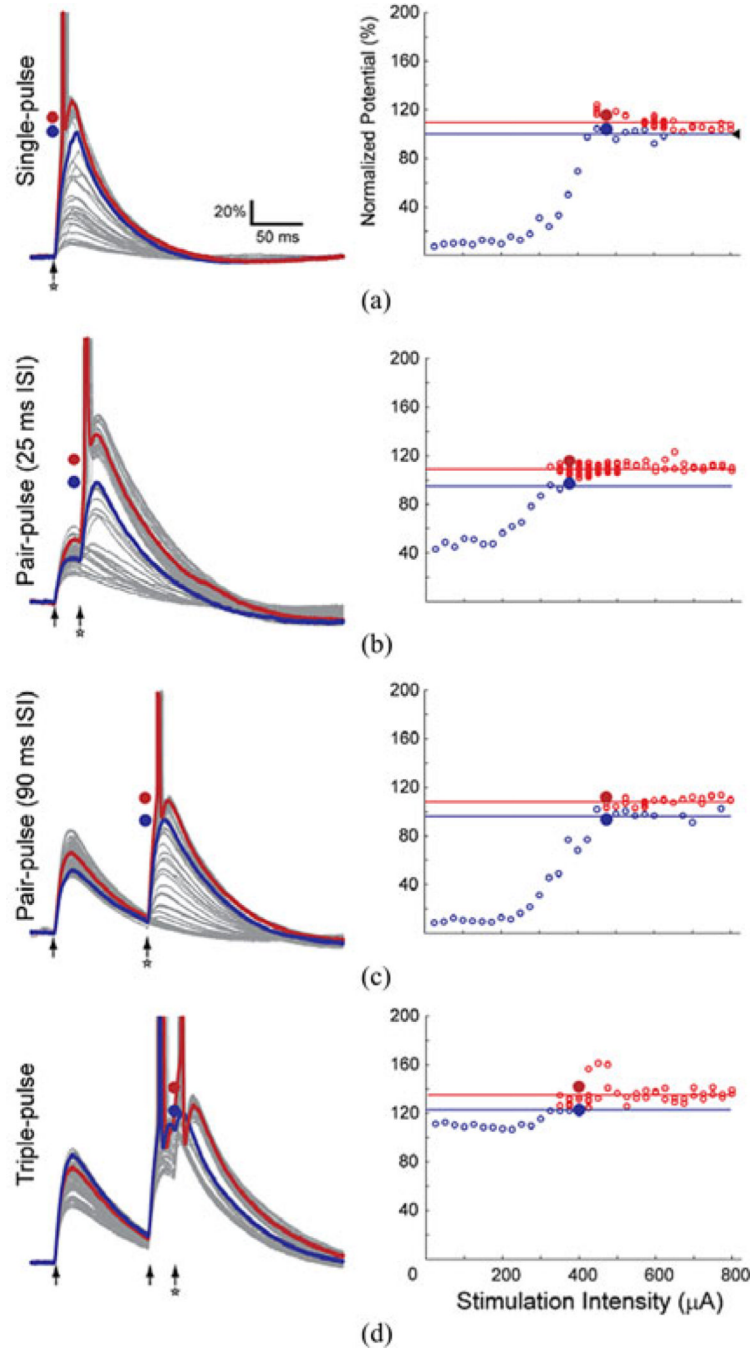


Fig. 5.

Four stimulation paradigms. (a) Single pulse, (b) pair pulse with a 25-ms ISI, (c) pair pulse with a 90-ms ISI, and (d) triple pulse with 90- and 25-ms ISIs in which an AP is induced by the second pulse and applied to examine 1) the consistency of the third-order derivative analysis in response to different membrane potential temporal patterns and 2) the relationship between AP turning point and neuron threshold. All data shown in Fig. 5 are from the same single neuron. All membrane potentials are normalized using the neuron threshold value (blue line) indicated by the black triangle (\blacktriangleleft) in the right panel of (a). In each panel on the left column, one representative nonspiking PSP response is highlighted with a blue color, and one representative spiking response is highlighted with a red color;

both highlighted responses are evoked using the same stimulation intensity. The peak value of the highlighted nonspiking PSP is labeled as a blue solid dot, and the AP turning point of the highlighted spiking response is labeled as a red solid dot. Arrows (\uparrow) indicate the stimulation timings. The star symbol indicates an increasing intensity stimulus ranging from 25 to 800 μA , which is the last stimulus in each paradigm. In each right neighboring panel, either the peaks (blue circles) of nonspiking responses or turning point values (red circles) of spiking responses induced by the last stimulus are plotted. The blue line indicates the average of the nonspiking peaks evoked with the stimulation intensities which also evoke spikes. Hence, this blue line represents the physiological neuron threshold. The red line is the average of all AP turning points. The red circles across different stimulation intensities show little variation. This shows that the third-order derivative analysis (see Fig. 2) provides consistent measurement of AP turning point in various temporal patterns of membrane potentials. The gap between the blue line and the red line represents the offset between AP turning point and neuron threshold. The offset remains relatively constant (10%) across all four stimulation paradigms. This indicates that the offset affects the first order (linear) but not the higher order (multiple preceding APs) response functions of threshold dynamics. Notice that the neuron threshold (blue line) and the AP turning point (red line) in (d) are roughly 20% larger than they are in (a), (b), and (c). This threshold elevation shows that the previous AP activity increases the threshold value for the following responses, and this effect is congruent with Figs. 3(b) and 6(b).

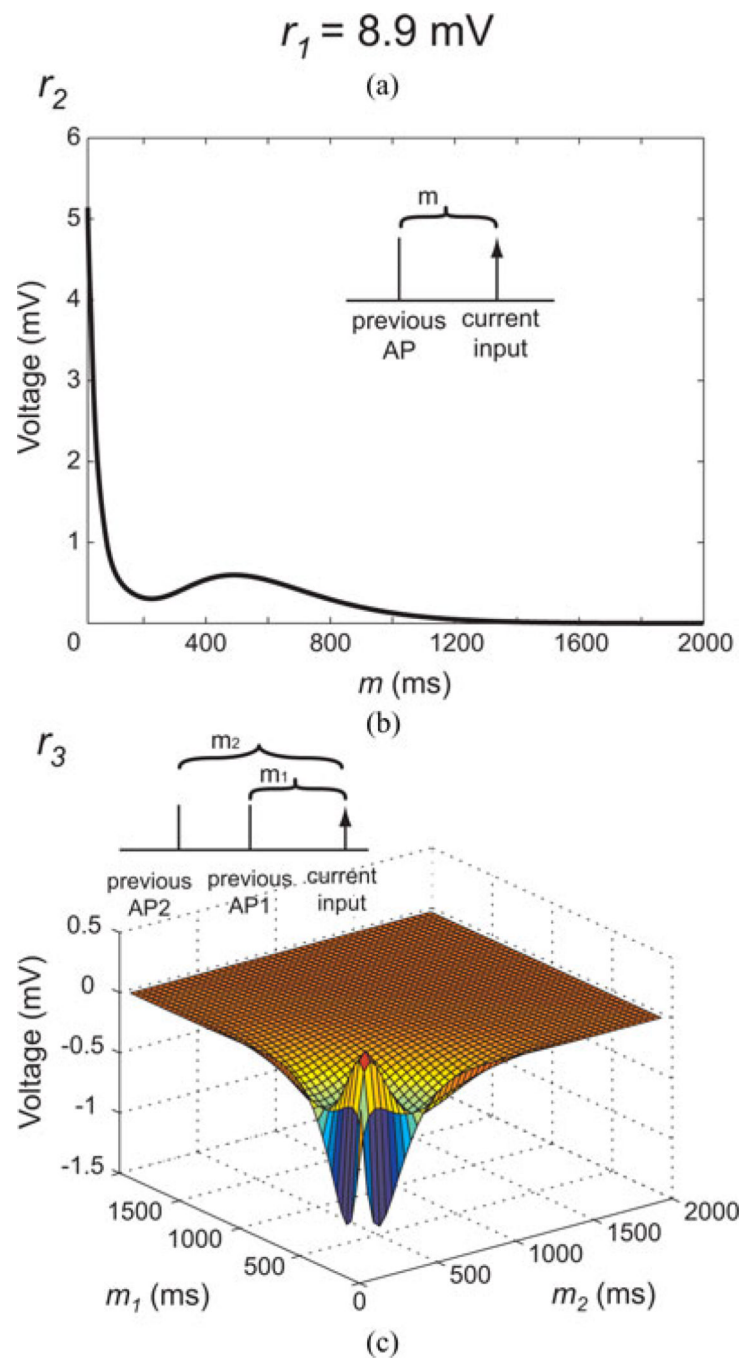


Fig. 6. Representative set of response functions of threshold dynamics. (a) First-order response function r_1 . (b) Second-order response function r_2 . (c) Third-order response function r_3 .

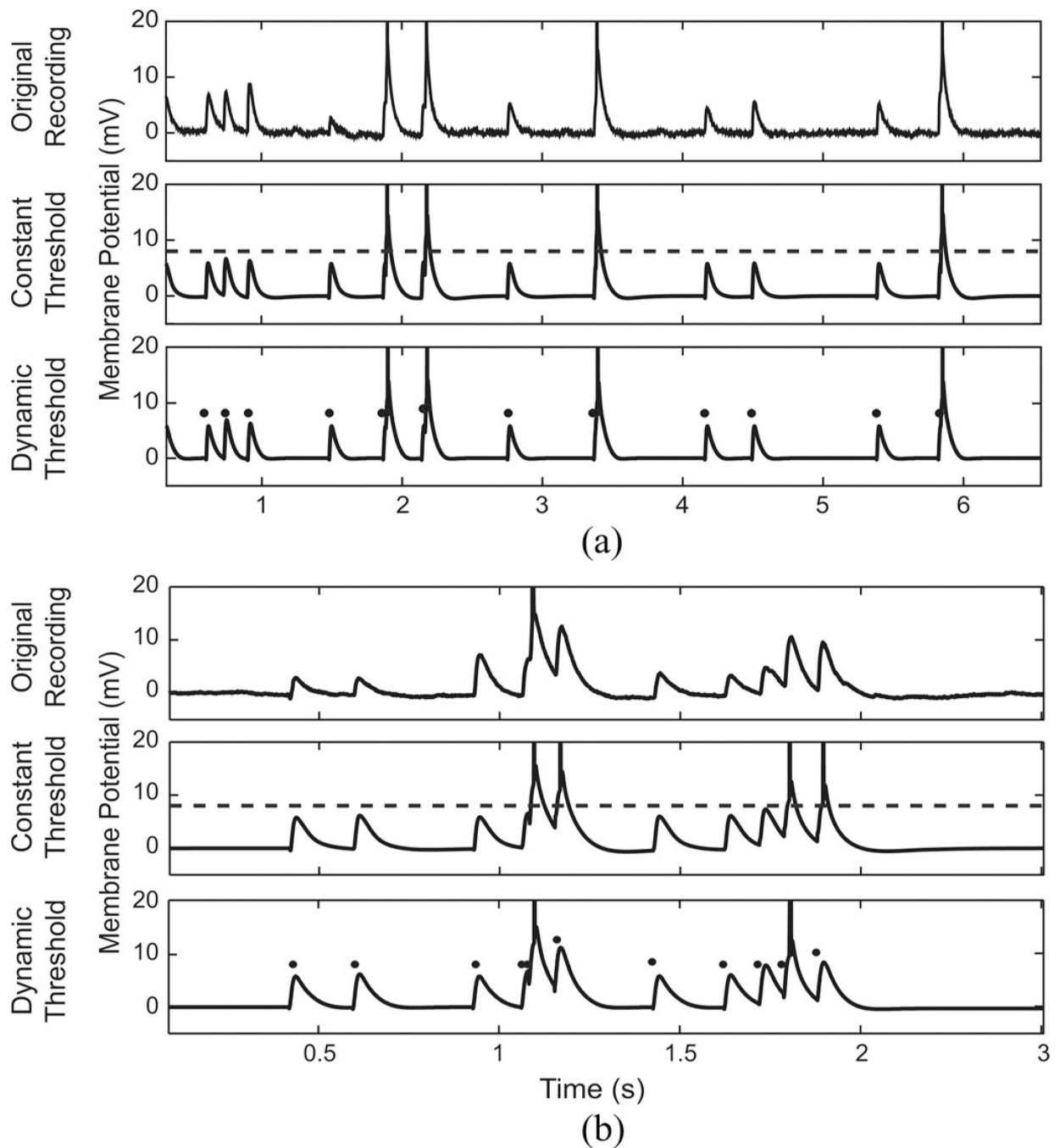
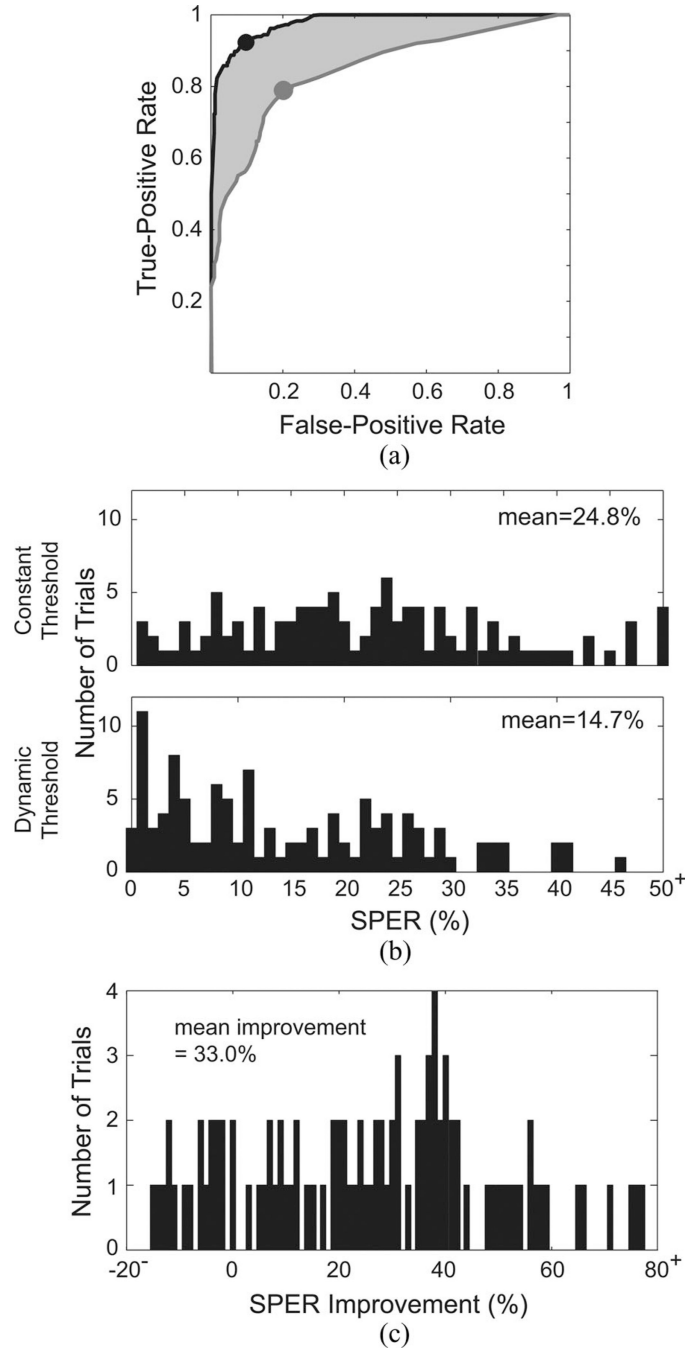


Fig. 7. Representative spike predictions performed using constant threshold and dynamic threshold. (a) When constant threshold worked perfectly, dynamic threshold worked just as well. (b) When constant threshold made three false-positive spike prediction errors, dynamic threshold avoided two of them and notably improved the prediction accuracy. In both (a) and (b), dashed lines in the middle panel indicate the optimal constant threshold; black dots in the bottom panels indicate varying threshold values predicted by the dynamic threshold model.

**Fig. 8.**

(a) Comparison of ROC curves. The black line is the spike prediction performances made using the dynamic threshold model with various offset values scanning through possible ranges. The black dot indicates the performance made using the optimal offset. The gray line represents the spike prediction performances made by various constant thresholds scanning through possible ranges. The gray dot indicates the performance made using the optimal constant threshold value. The gray shadow area indicates the improvement in spike prediction made using the dynamic threshold versus constant threshold. (b) SPERs made by the single neuron model with the optimal constant threshold and the dynamic threshold. (c)

Average of 33.0% improvement in SPER was observed by using the dynamic threshold model over a constant threshold.